ICAS 2020 SHANG HAI
International Council of the Aeronautical Sciences
32nd Congress of the International Council of the Aeronautical Sciences
September 6-10, 2021
Pudong Shangri-La, Shanghai, China

# MEASUREMENT AND ANALYSIS OF INTER-STAGE FLOW FIELD IN A HIGH-LOAD AXIAL MULTISTAGE COMPRESSOR

Zhang Zhibo, Gao Feilong, Wu Hui, Chen Yehui

AECC Shenyang Engine Research Institute, Shenyang 100015, China

## Abstract

The inter-stage flow fields of a full-scale four stage compressor at different working conditions were measured in detail by blade profile probe, five-hole probe and high-frequency dynamic probe. The pressure, temperature and Ma distributions after each stage rotor were quantitatively analyzed, and the flow mechanism affecting the compressor performance was diagnosed. It provides data and theoretical basis for the optimal design of multistage compressor. The results show that by using the customized small-size L-shaped five-hole probe and high-frequency dynamic single-hole probe, the measurement problems caused by the narrow space of full-size multistage compressor can be well overcome, and detailed distribution of flow field parameters after the rotor blade along the radial and circumferential directions can be measured. Through the comparison and analysis of the overall performance, stage performance and inter-stage flow field, the main separation characteristics near the end wall affecting the compressor performance are effectively diagnosed.

**Keywords:** axial-flow multistage compressor; inter-stage flow field; flow field diagnosis; steady-state five-hole probe; high-frequency dynamic single hole probe.

## 1. General Introduction

The compressor of an aero engine is generally composed of multiple stages, and a high-performance multi-stage compressor requires the blades of each stage to be matched in a better working condition. However, in the compressor, there are various complex secondary flows, such as tip leakage flow, Interaction between shock wave and boundary layer, corner separation, etc. These flows will destroy the matching between the blades of each stage, resulting in the decrease of compressor pressurization capacity and the increase of compressor loss [1-8]. Therefore, it is very important for compressor performance diagnosis to analyze the real flow inside the compressor and find out the influence of flow field on matching.

Since the 1990s, CFD technology has developed rapidly, and has become the main tool to study the complex flow inside the compressor. However, due to the characteristics of CFD technology, its simulation accuracy is affected by many factors, such as the choice of turbulence model, mixing surface and near wall treatment [9-12]. Especially for multistage axial compressor, the internal flow of the compressor has strong three-dimensional and strong unsteady characteristics, and has strong upstream and downstream interaction. It is difficult for CFD to simulate the complex flow in this multi-stage environment. Therefore, it is still necessary to obtain the real flow situation in the compressor through experiments and analyze the physical mechanism restricting the compressor performance.

Over the years, many scholars have carried out a lot of work on the test of complex flow field in low-speed large-scale compressor, and applied many advanced test technologies, including steady-state pressure probe, dynamic pressure probe, hot wire, PIV (particle image velocimetry), LDA (laser Doppler velocimeter), and achieved good application results [13-19]. However, in the engineering field, a full-scale multi-stage compressor has short axial length, small blade size, narrow axial spacing between blade rows, and the casing is usually equipped with an actuator with adjustable stator blades. Therefore, it is extremely difficult to carry out internal flow field testing. Common testing methods on low-speed large-scale compressor, such as PIV, LDA, hotline, etc., are difficult to apply to full-scale multi-stage compressors. At present, the contact probe is still the

most mature and reliable way to test the flow field in a full-scale compressor. Kupferschmied et al. used a dynamic probe to measure the detailed flow field on a high-speed turbomachine [20]. Ma Hongwei et al carried out an experimental study on a transonic compressor using a probe with the dynamic sensor embedded in the probe head [21-23]. However, due to the narrow space and complex structure of full-scale compressor, the probe should not only ensure small size, but also overcome the test difficulties caused by vibration and high temperature.

In this paper, the temperature, pressure, Ma and other parameters of a full-scale multistage axial flow compressor are measured, and the main factors affecting the compressor performance are analyzed. It is hoped that through experimental testing methods, the real inter-stage flow field inside the compressor can be obtained, so as to provide data and theoretical basis for the optimization of multi-stage compressors.

## 2. Experimental Compressor and Test Device

### 2.1 Experimental Compressor

This four-stage axial compressor (HLC86) has 9 rows of blades including the inlet guide vanes. The compressor flow path is shown in Figure 1. The inlet guide vanes, the first and second stage stators are all adjustable stator blades. Therefore, the casing of the compressor is very complicated, which brings great difficulties to the inter-stage flow field test. In addition, the full-size compressor has narrow blade size and blade row spacing, high speed, high blade passing frequency, and complex flow field, which further increases the difficulty of the inter-stage flow field measurement.

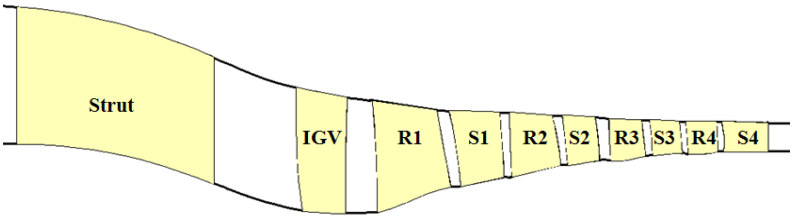


Figure 1 – Compressor flow path diagram

### 2.2 Test Device

The test device is shown in Figure 2, which is composed of power system, air intake system, exhaust system, lubricating oil system, electrical system, measuring system, etc. During the test, the gas flows through the inlet flow tube, the front diffuser, the intake throttle, the diffuser and the pressure stabilizing box. After rectifying by the honeycomb and the rectifying net of the pressure stabilizing box, it enters the compressor through the bell mouth, and finally the air flow is discharged through the exhaust system.

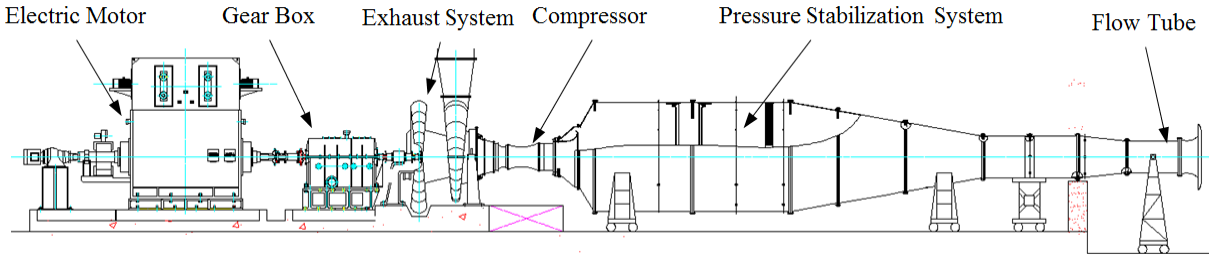


Figure 2 – Schematic diagram of compressor test device

## 3. Test Equipment and Method

### 3.1 Measuring equipment

#### *3.1.1 Steady state data acquisition system*

During the compressor test, the steady-state pressure signal is collected by the pressure scanning valve DSA3217, with an accuracy of ±0.05% F.S. The compressor inlet temperature test equipment is Ex1000A, and the data acquisition accuracy of the equipment is ±0.3K. The outlet temperature measuring equipment is Ex1000A-TC, when the temperature is below 300℃, the data acquisition accuracy of the equipment is ±0.2K. The torque and speed are measured by an ET1200HS torque measuring instrument, and the speed measurement accuracy is ±1rpm.

### *3.1.2 Pulsating pressure data acquisition system*

The dynamic data test and analysis system based on the PXIE6356 acquisition board produced by NI Company can realize data acquisition with a maximum sampling frequency of 500 kHz. During the test, a square wave trigger signal is provided by the rotational speed measurement system to achieve phase-locked acquisition.

## 3.2 Overall Performance Test Method

In order to obtain the compressor overall performance, it is necessary to measure the inlet mass flow, inlet and outlet temperature and pressure. The mass flow of the compressor is measured by the flow tube, which is arranged in front of the pressure stabilizing box of the test device (as shown in Figure 2). The physical flow is calculated by measuring the total pressure, total temperature and wall static pressure of the flow tube.

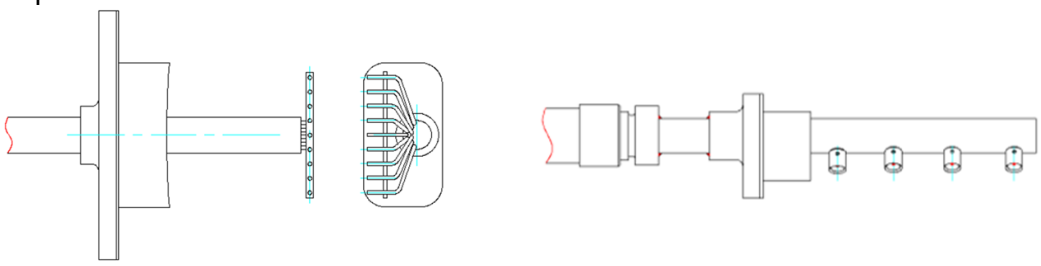

(a) Rake-shaped total pressure probe (b) Comb-shaped total pressure/temperature probe

Figure 3 – Schematic diagram of pressure and temperature test instrument

The total pressure at the compressor inlet is obtained by using two 5-point comb-shaped total pressure probes arranged in front of the guide vane. Six 4-point comb-shaped probes and four 9-point rake-shaped probes were used to measure the temperature and pressure at the compressor outlet (as shown in Figure 3). To judge the surge boundary, the pressure pulsation is measured at the compressor outlet and the stall or surge of the compressor is judged according to the pulsation characteristics.

## 3.3 Inter-stage Flow Field Test Method

### *3.3.1 Blade profile probe test method*

In order to measure the temperature and pressure fields between stages, the total temperature and total pressure blade profile probes are arranged after the rotor blades of each stage. The structure and arrangement of the blade profile probes are shown in Figure 4. After the first and second stage rotors, the blade profile probe has six radial measuring points (located at 16%, 31%, 46%, 60%, 74% and 87% blade height respectively), and after the third and fourth stage rotors, the blade profile probe has five radial measuring points (located at 17%, 35%, 51%, 68% and 84% blade height respectively).

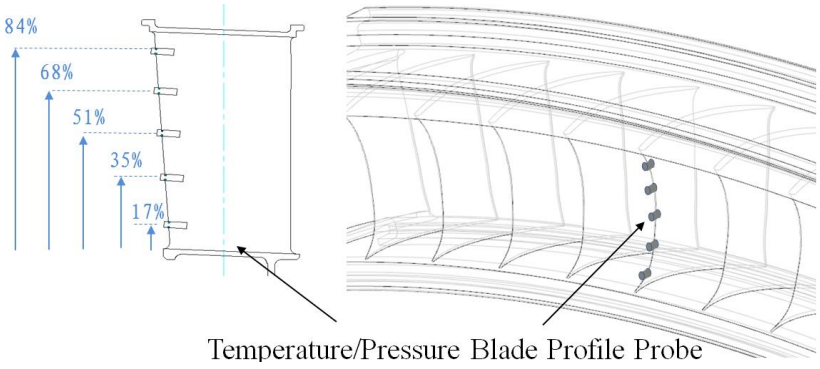


Figure 4 – Schematic diagram of blade profile probe

### *3.3.2 Five-hole probe test method*

In order to obtain the flow capacity between stages, a customized five-hole probe is used to measure the steady flow field after the second and third stage rotors at the design speed. The test sections are shown in Figure 5.

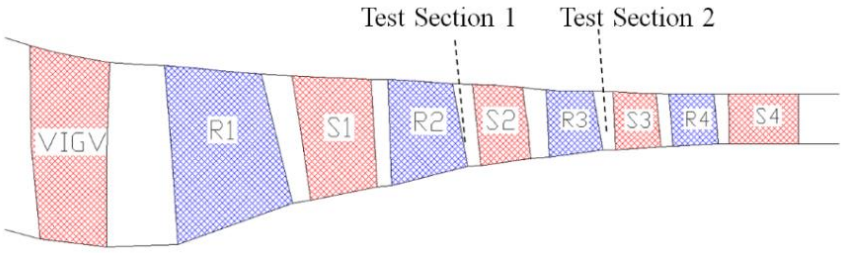


Figure 5 – Test section of steady state five-hole probe and dynamic single-hole probe

Due to the complex mechanical structure, narrow row spacing (about 7 mm-9 mm) and short blade height (about 25 mm-40 mm) of the full-scale compressor, as shown in Figure 6, it is very difficult to use probe measurement. Therefore, according to the compressor structure, a five-hole probe with high precision and small size is customized. The probe is L-shaped (as shown in Figure 7), the diameter of the probe rod is 6 mm, the head is conical (about 2 mm in diameter), and the probe head does not exceed the projection range of the probe rod diameter, which is convenient to change the radial position of the probe head in the narrow space between stages.

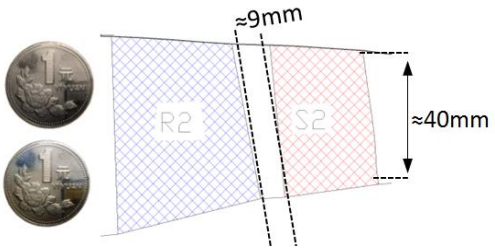


Figure 6 –Schematic diagram of the second stage blade size

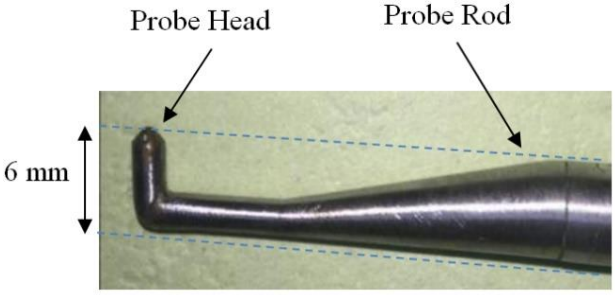


Figure 7 –Customized L-shaped five-hole probe

Since the second-stage stators are an angle-adjustable blades, in order to avoid collision between the probe and the stator blade, the leading edge of the blade nearest to the probe is cut off by 1 / 3 of the blade chord length. The position of the probe head relative to the blade is shown in Figure 8.

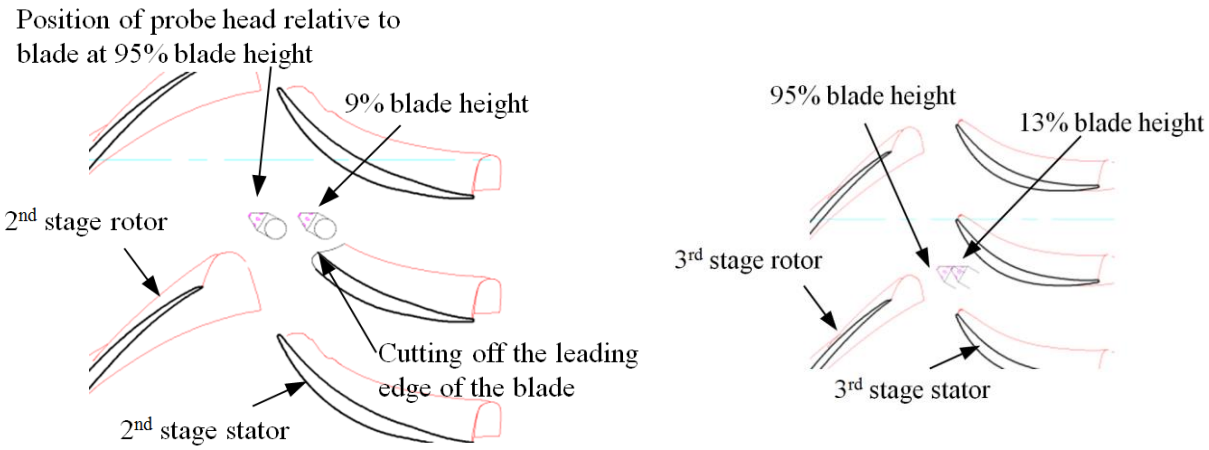


(a) the second stage (b) the third stage

Figure 8 –Position of probe head relative to blade at different blade height

### *3.3.3 Dynamic single-hole probe test method between stages*

Although the five-hole probe can obtain the circumferential average aerodynamic parameters at different blade heights after the rotor blade, the circumferential distribution of the flow cannot be analyzed. In order to further qualitatively analyze flow field distribution of the S3 stream surface, the dynamic probe is used to measure the flow field after the second and third stage rotors, and the test section is shown in Figure 5.

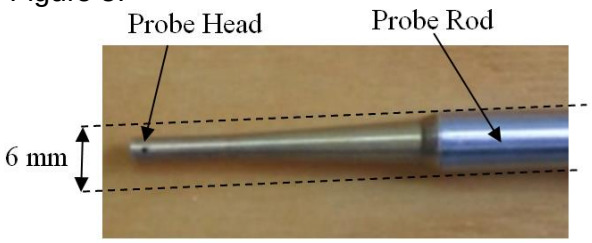


Figure 9 –High frequency dynamic single hole probe

In order to adapt to the characteristics of narrow compressor geometry and high blade passing frequency, a high frequency dynamic single hole aerodynamic probe is customized (as shown in Figure 9). The pressure measuring hole is located on the side of the probe head, and a micro dynamic pressure sensor is installed in the probe head to collect the dynamic pressure signal of the flow field. The size of the probe head is about 2 mm, the diameter of the probe rod is 6 mm, and the comprehensive response frequency of the dynamic probe and the measurement system is about 60 kHz. Similar to the steady-state five-hole probe, the probe head does not exceed the projection range of the probe rod diameter. By rotating the probe head, the dynamic single hole probe can get the pressure of multiple directions, and then according to the calibration data, the Ma, pressure and other aerodynamic parameters can be obtained.

Phase locked measurement is used in the test process. When the measurement system receives the trigger signal, a group of dynamic signal measurement is completed within one revolution of the compressor, and 100 groups of dynamic data are collected for each experimental condition. Through the average treatment, the flow field distribution of S3 stream surface after the rotor is obtained as shown in Figure 10.

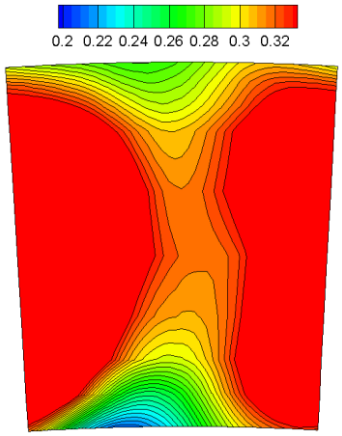


Figure 10 –The distribution of Ma after rotor measured by dynamic probe

## 4. Test Results and Analysis

### 4.1 Compressor overall performance at design speed

Figure 11 shows the overall performance of the compressor at design speed including design condition (De), intermediate condition (Mid01 and Mid02) and near surge condition (Ns). The flow rate, pressure ratio and efficiency in the figure are normalized based on the performance of De condition.

It can be seen from the figure that the compressor is close to the highest efficiency state at De condition. As the flow rate decreases further, the pressure ratio increases slowly and the efficiency gradually decreases. Compared with the De condition, the pressure ratio at Ns condition is increased by about 5%, and the efficiency is reduced by about 4%. Compared with the CFD simulation results, the overall characteristics are quite different. The flow rate of the compressor at

Ns condition is about 5% lower, and the maximum efficiency is about 4% lower, indicating that the actual flow field matching of the compressor is quite different from the CFD simulation results.

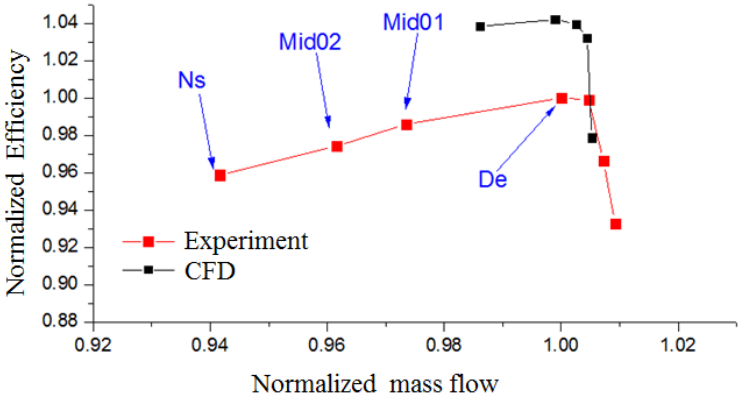


(a) Pressure ratio characteristic

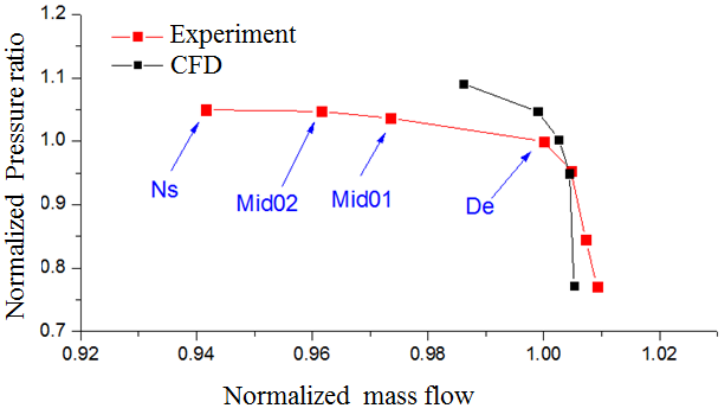


(b) Efficiency characteristic

Figure 11 –Overall performance of compressor at design speed

## 4.2 Stage performance design speed

According to the total temperature and total pressure measured by the blade profile probe, the pressure ratio and efficiency characteristics between the two rows of stators can be obtained. When analyzing the stage performance, the definition of each stage is shown in Figure 12. The first stage is IGV + R1, the second stage is S1 + R2, the third stage is S2 + R3, and the fourth stage is S3 + R4.

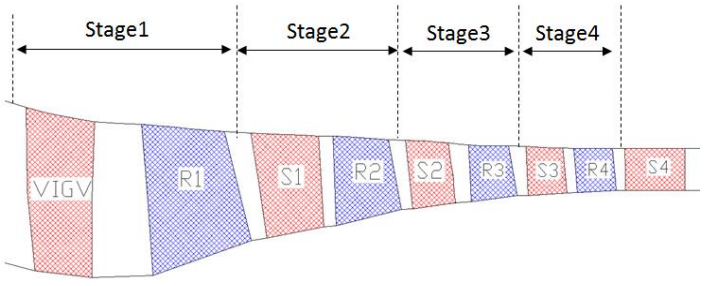


Figure 12 –The definition of each stage of the compressor

The pressure ratio and efficiency characteristics of each stage are shown in Figure 13-14, in which the performance of De, Mid01, Mid02 and Ns operating points are identified. In order to compare the four stage characteristics conveniently, the flow rate in the figure adopts the compressor inlet flow rate. When calculating the pressure ratio and efficiency, the measured temperature and pressure data are processed by area weighted average. The flow rate, pressure ratio and efficiency of each state are normalized based on the first stage performance of De condition.

It can be seen from Figure 13(a) that from De to Ns condition, the pressure ratio of the first and second stage increases gradually, especially the pressure ratio of the first stage increases most obviously with the decrease of flow rate. At Ns condition, the pressure ratio of the first stage

increases by about 3.5% compared with De condition, and the pressure ratio of the second stage blade increases by about 2.3%. However, the pressure ratio of the third and fourth stage blades is almost constant with the decrease of flow rate from De to Ns condition.

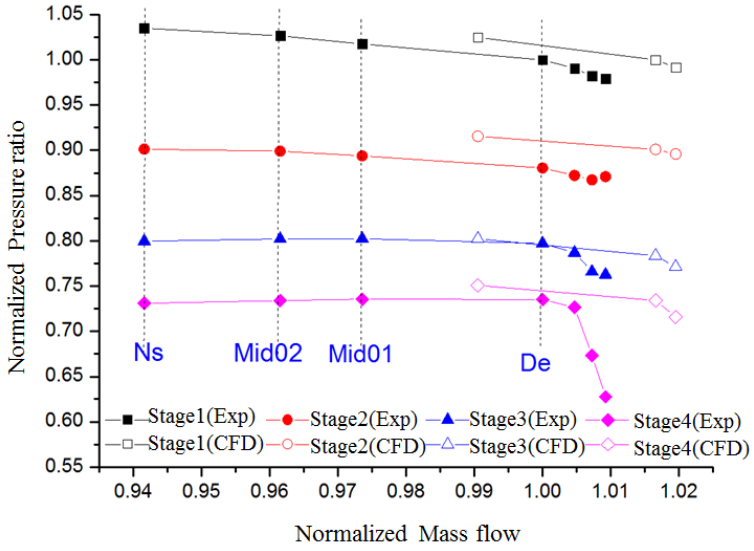


(a) Pressure ratio characteristic

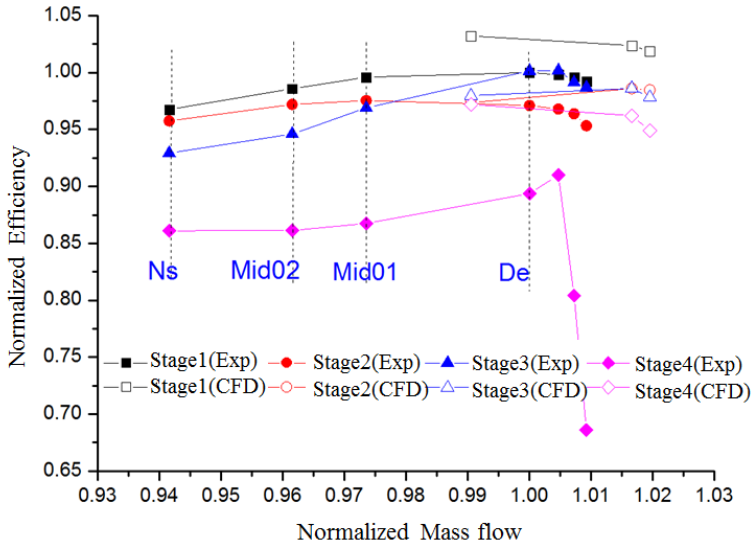


(b) Efficiency characteristic

Figure 13 –Stage performance of compressor at design speed

As shown in Figure 13(b), the efficiency of each stage is lower than the CFD simulation results, and the efficiency of the first three stages is significantly higher than that of the fourth stage. With the decrease of flow rate, the efficiency of each stage decreased gradually, and the second stage changed the least, and the third stage decreased the most. Compared with De condition, the efficiency of the first stage to the fourth stage decreased by 3.5%, 1.4%, 7% and 3.3% respectively at Ns condition.

In conclusion, the pressure margin of each stage is mainly provided by the first and second stages, and the stage efficiency is higher; However, the third and fourth stages are in poor matching state, and there is almost no change in supercharging capacity after De condition, especially the efficiency of the fourth stage is significantly lower than that of the first three stages

## 4.3 Inter-stage flow field at design speed

### *4.3.1 Radial distribution of interstage pressure ratio and efficiency*

Figures 14 shows the radial distributions of the pressure ratio and efficiency after rotors at De, Mid01, Mid02 and Ns conditions. The pressure ratio and efficiency are normalized by the stage average pressure ratio and average efficiency at De condition.

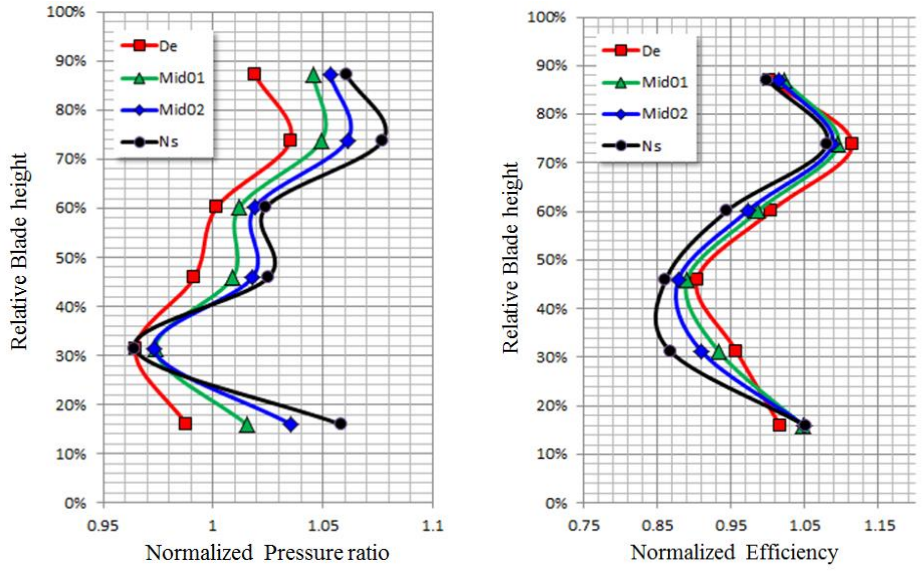


(a) Flow field after the first stage rotor

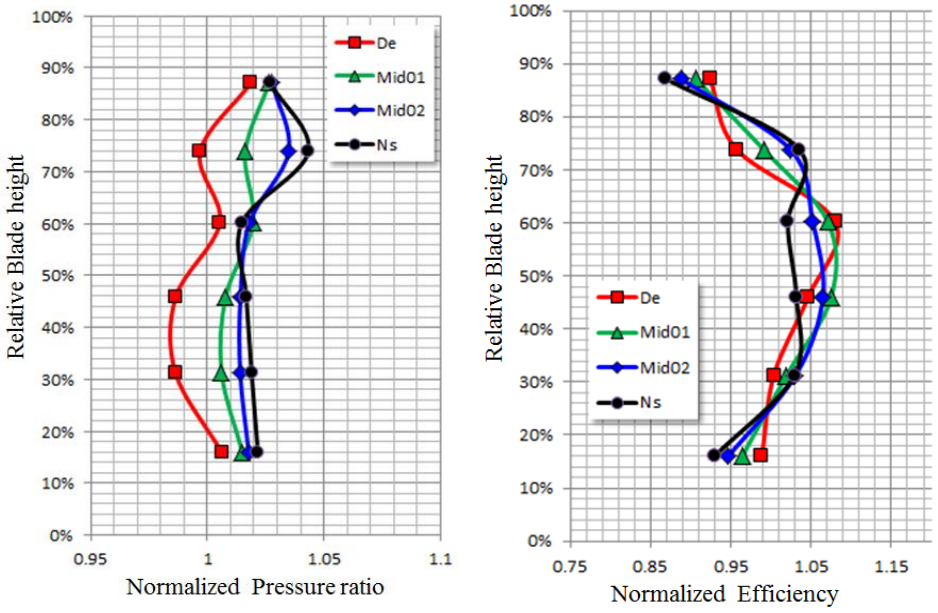


(b) Flow field after the second stage rotor

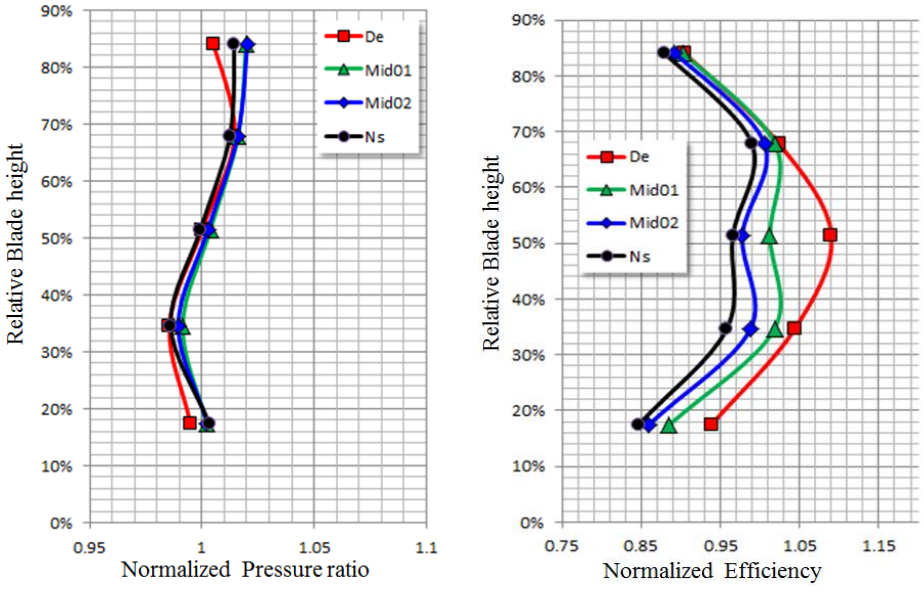


(c) Flow field after the third stage rotor

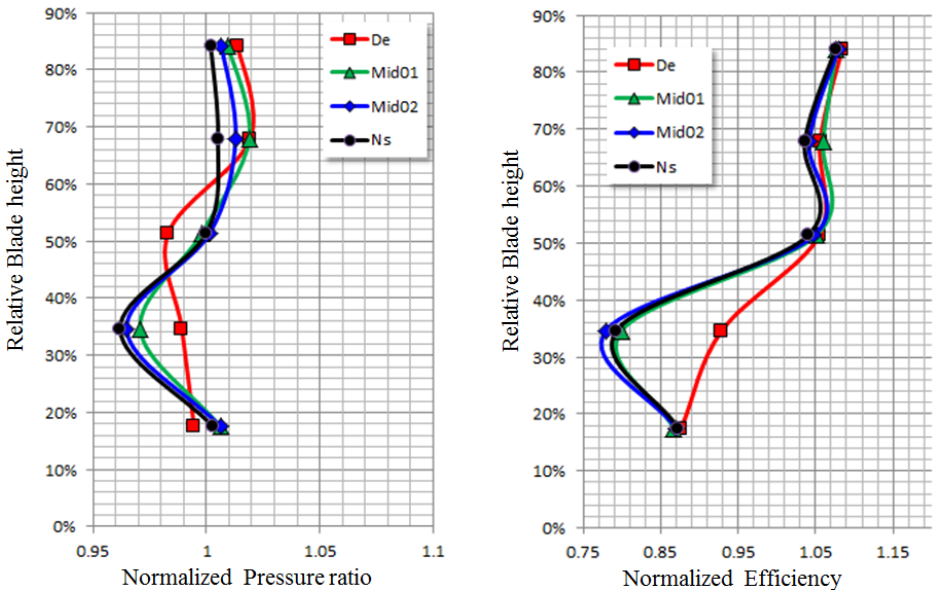


(d) Flow field after the fourth stage rotor

Figure 14 –Distribution of single stage pressure ratio and efficiency along radial direction after each stage rotor at deign speed

It can be seen from Figure 14 (a) that for different working conditions, the pressure ratio of the first stage shows a strong pressurize ability near the tip, the pressurize ability is the strongest and the efficiency is the highest near 74% blade height, and the pressurize ability is the weakest and the efficiency is the lowest near 31% blade height. From De to Ns condition, except around 31% blade height, the pressure ratio increases gradually, while the change of pressure ratio at 31% blade height is small.

It can be seen from Figure 14 (b) that the pressure ratio after the second stage rotor is evenly distributed along the blade height, and the variation along the radial distribution is not more than 3.5%. The highest efficiency is near the middle blade, and the efficiency decreases near the hub and casing. From De to Ns condition, the pressure ratio near the end wall (87% and 16% blade height) does not change significantly, and the efficiency decreases gradually with the state approaching the surge boundary. In the mainstream region (31%-74% blade height), except that the pressure ratio at 60% blade height does not change significantly with the working conditions, the pressurization capacity increases with the decrease of inlet flow rate, especially at 74% blade height, the pressure ratio increases most significantly and the efficiency increases by about 8%.

It can be seen from Figure 14 (c) that the overall distributions of the flow after the third stage rotor are relatively uniform at different working conditions, the pressure ratio at the rotor tip is slightly larger, and it is the minimum at 35% blade height. The efficiency near the middle blade height is the highest, and the closer to the end wall, the lower the efficiency. The results show that with the decrease of the inlet flow rate, the pressurization capacity of the stage is almost not improved, but the efficiency of the lower half of the blade decreases significantly. Especially at Ns condition, the efficiency of the middle and root regions of the blade decreases by about 12.5% and 9% respectively compared with the De condition. It shows that the flow in the lower half of the third stage blade is easy to separate and cause significant flow loss.

It can be seen from Figure 14 (d) that with the decrease of flow rate, the performance of the lower half of blade height decreases obviously, especially near 35% blade height, the pressurization capacity decreases by about 2%-3% at Ns condition, and the efficiency decreases sharply by about 13.5%, which indicates that the flow of this stage is significantly worse than that of the first three stages, especially near the blade root.

According to the single-stage performance of each stage blade and the radial distribution of pressure ratio and efficiency after the rotor blade, the flow matching of the third and fourth stage blades is poor, and the flow loss is significant.

### *4.3.2 Axial Ma distribution between stages*

Five-hole probe and dynamic single hole probe were used to measure the flow field after the second and third stage rotors. Because it takes a long time to measure the inter-stage flow fields with the probe, and the aerodynamic state of the compressor cannot be stable for a long time at Ns condition, only the flow field results at De, Mid01 and Mid02 conditions were measured to analyze the flow capacity between stages.

Figure 15 shows the distribution of axial Ma along the blade height measured by the five-hole probe, and normalized by the area weighted average axial Ma at De condition. After the second stage rotor, the flow field at 9%-95% of the blade height was measured, and after the third-stage rotor, the flow field at 13%-95% of the blade height was measured.

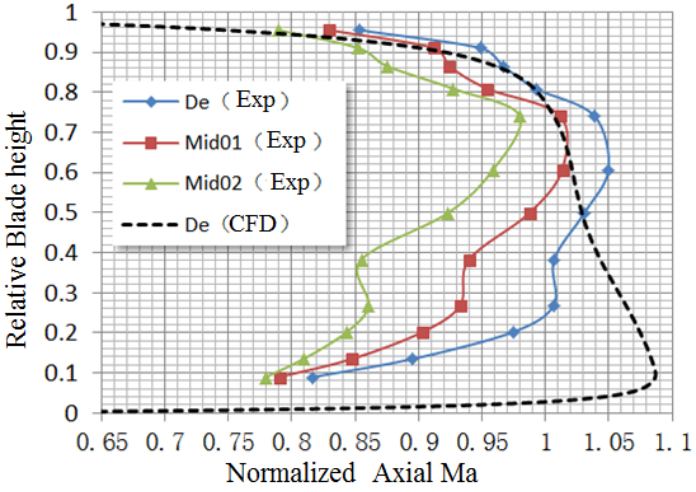


(a) Flow field after the second stage rotor

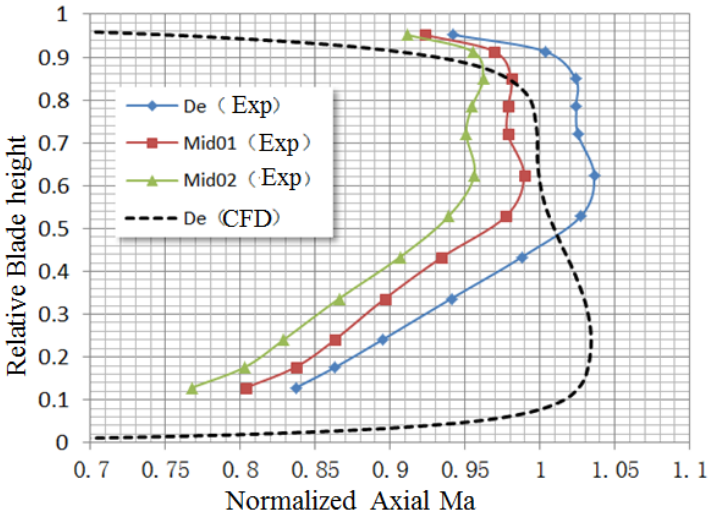


(b) Flow field after the third stage rotor

Figure 15 –Distribution of normalized axial ma after second and third stage rotor measured by five-hole probe

It can be seen from Figure 15(a) that the CFD result after the second stage rotor at De condition is that the axial Ma near the blade root is higher, which means the flow capacity at the blade root is stronger, and it gradually decreases from the root to the tip. However, the experimental and CFD results are quite different. The experimental results show that the axial Ma in the main flow region (about 25%-70% blade height) is more uniform, and the variation is less than 5%. The axial Ma near the hub (about 70% blade height above) and near the casing (about 25% blade height below) is lower, which indicates that the flow is blocked in the near end wall region. With the decrease of the flow rate, the axial Ma of the near end wall region decreases further, especially the area close to the hub.

It can be seen from Figure 15 (b) that the axial Ma distributions after the third stage rotor are very similar for different conditions. The axial Ma distribution is relatively uniform from 50% to 90% of the blade height, and the variation is less than 3.5% Or less, but near the casing (above about 90% blade height) and near the hub (about 50% blade height below), the axial Ma has a significant tendency to decrease, and there is a strong flow blockage.

Figure 16-17 shows the axial Ma distributions after the second and third stage rotors measured by the dynamic single hole probe, and normalized using the same method as the measurement result of the five-hole probe. The flow field at 10%-95% blade height is measured after the second stage rotor, and the flow field at 17.5%-62.5% blade height is measured after the third stage rotor.

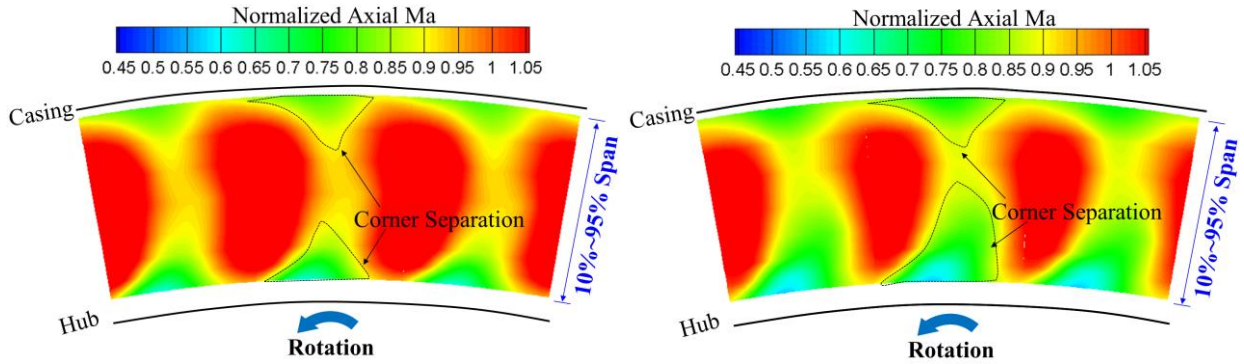


(a) De condition (b) Mid02 condition

Figure 16 –Distribution of normalized axial ma after second stage rotor measured by dynamic probe

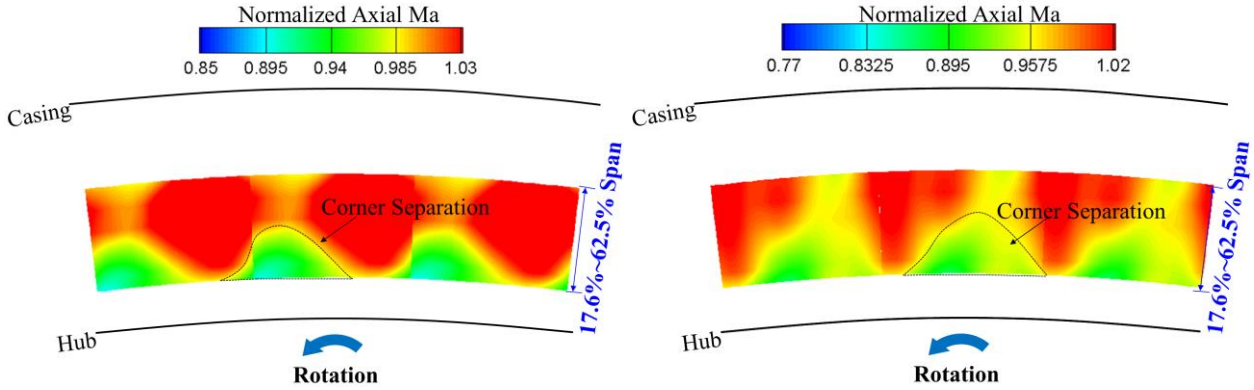


(a) De condition (b) Mid02 condition

Figure 17 –Distribution of normalized axial ma after third stage rotor measured by dynamic probe

The axial Ma distribution after the second stage rotor shows that there is obvious flow blockage near the hub and casing caused by secondary flow. The size of the separation zone near the hub is slightly stronger than that near the casing at De condition. When the flow rate decreases to Mid02 condition, the size of the separation zone near the hub expands to more than the middle of the blade, indicating that the separation at the blade root is significantly enhanced, which is consistent with the distribution obtained by the five-hole probe.

The axial Ma distribution after the third stage rotor shows that there is a large-scale low Ma region near the hub at De and Mid02 conditions, which indicates that there is a strong flow separation. Compared with the De condition, the separation scale at Mid02 condition increases slightly along the circumferential and radial direction.

By comparing the measurement results of the blade profile probe, the steady-state five-hole probe and the dynamic probe, the flow mechanism affecting the compressor performance can be analyzed. The results show that there is flow separation at 30% blade height of the first stage, but it still has strong pressurization capacity. For the second stage, there is a certain degree of flow separation near the hub and the casing, which leads to the decrease of the flow capacity near the end wall and the increase of the flow loss. As the inlet flow rate decreases from De to Ns condition, the separation zone near the hub expands rapidly to the region above the middle of the blade. For

the third stage, the total pressure and Ma of the upstream near wall region are lower, which leads to the increase of incidence and stronger flow separation in the downstream. With the decrease of the inlet flow rate, the flow in the near wall region deteriorates further, and the flow loss increases significantly, which limits the pressurization capacity of the third stage, indicating that the third stage blade always matches in a poor working condition; Due to the flow separation near the hub of the third stage blade, the flow state of the downstream fourth stage blade is further deteriorated, the flow separation is strengthened, and the loss increases sharply.

## 5. Conclusion

In this paper, the inter-stage flow fields of a full-scale four-stage axial compressor are measured. Through the analysis of the overall performance, stage performance and inter-stage flow, the following main conclusions are obtained:

(1) the circumferential average pressure and temperature distributions at different blade heights after the rotor blades were successfully measured by arranging pressure and temperature blade profile probes with multiple measuring points, and each stage performance of the compressor was obtained.

(2) By using customized small L-shaped five-hole probe and high frequency dynamic single hole pressure probe, the problem of narrow measurement space between compressor stages is overcome, the high spatial resolution and high frequency measurement of flow field between stages are realized, and the detailed flow fields distribution of S3 stream surface are obtained

(3) The main characteristics of flow separation near the end wall, which affect the performance of the compressor, and the influence on the performance of the upstream and downstream blades can be effectively diagnosed through the comprehensive comparison and analysis of the compressor overall performance, stage performance and inter-stage flow field.

## 6. Contact Author Email Address

Mailto: zhibo346@163.com

## 7. Copyright Statement

## References


[1] Papalia J, Lawless P B, Fleeter S. Off-design transonic rotor-inlet guide vane unsteady aerodynamic interactions. Journal of Propulsion and Power, Vol. 21, No. 4, pp 715-727,2005

[2] Koch C C. Stalling pressure rise capability of axial flow compressor stages. ASME Journal of Engineering for Power, Vol. 103, No. 4, pp 645-656, 1981.

[3] Venter S J, DG Kröger. The effect of tip clearance on the performance of an axial flow fan. Energy Conversion and Management, Vol. 33, No.2, pp 89-97, 1992.

[4] Wisler D C. Loss reduction in axial-flow compressors through low-speed model testing. ASME J.Eng. Gas Turbines and Power, Vol.107, No.2, pp 354-363, 1985.

[5] Baghdadi S. Modeling tip clearance effects in multistage axial compressors. Journal of Turbomachinery, Vol.118, No.4, pp 613-843, 1996.

[6] Sanders A J, Hassan K K, Rabe D C. Experimental and numerical study of stall flutter in a transonic low-aspect ratio fan blisk. Journal of Turbomachinery, Vol.126, No.1, pp 166-174, 2004.

[7] Koch C C, Smith L H. Loss sources and magnitudes in axial-flow compressors. Journal of Engineering for Power, Vol.98, No.3, pp 411-424, 1973.

[8] Khalid S A, Khalsa A S. Endwall blockage in axial compressors. Journal of Turbomachinery, Vol.121, No.3, pp 499-509, 1999.

[9] Denton J D. Some limitations of turbomachinery CFD. ASME Turbo Expo Power for Land Sea & Air, Glasgow, No.GT2010-22540, pp 735-745, 2010.

[10] LIU Yangwei, YU Xianjun, LIU Baljie. Turbulence models assessment for large-scale tip vortices in an axial compressor rotor [J], Journal of Propulsion and Power, Vol.24, No.1, pp 15-25, 2008.

[11] Yan Fei, LIU Yang Wei, LU Li Peng. Modification of realizable $\kappa$ - $\varepsilon$ model for tip-leakage flow in an axial compressor rotor. Journal of Engineering Thermophysics, Vol. 40, No. 3，pp 505-512, 2019.

[12] CHEN Maozhang, LIU Baojie. Fan/compressor aero design trend and challenge on the development of high bypass ratio turbofan. Journal of Aerospace Power, Vol. 23, No.6，pp 961-975, 2008.

[13] LIU Bao Jie YU Hong Jun LIU Huo Xing JIANG Hao Kang. Measurement of compressor rotor tip leakage vortex with SPIV, Journal of Engineering Thermophysics, Vol. 25 No. 5，pp 67-72, 2016.

[14] Yu Xianjun, Liu Baojie, Jiang Haokang. Three-dimensional flows near rotor tip in an axial compressor Ⅰ -experimental and theoretical studies. Acta Aeronautica Et Astronautica Sinica, Vol. 42 No. 2, pp 67-72，2016.

[15] Zhang Z B, Xian J Y, Liu B J. Characteristics of the tip leakage vortex in a low-speed axial compressor with different rotor tip gaps. ASME Turbo EXPO, Copenhagen, GT2012-69148, pp 311-322, 2012.

[16] LIU Baojie, ZHANG Zhibo, YU Xianjun. Experimental investigation on characteristics of tip leakage blockage in an axial compressor. Acta Aeronautica et Astronautica Sinica, Vol. 34 No. 12，pp 2682-2691，2013.

[17] XU Yueting, JIANG Haokang. 3-D LDV measurements for the flow in rotor tip region of a compressor, Journal of engineering thermophysics, Vol. 19, No. 2, pp 175-179, 1998.

[18] LIU Baojie, ZHANG Shuai, YU Xianjun, AN Guangfeng, FU Danyang. Optimization design of a single stage low speed simulation axial compressor test facility. Journal of Aerospace Power, Vol. 33, No. 7, pp 1665-1675, 2018.

[19] MA Hong wei, JIANG Hao kang. 3-D turbulent characteristics of the tip leakage vortex inside an axial compressor rotor passage at a low mass-flow condition. Journal of Aerospace Power, Vol. 15, No. 4, pp 347-352, 2000.

[20] Kupferschmied P, Koppel P，Gizzi W，et al. Time-resolved flow measurements with fast-response aerodynamic probes in turbomachines. Measurement Science Technology, Vol. 11, No. 7, pp 1036-1054, 2000.

[21] MA Hong wei, HE Xiang, SHAN Xiao ming, YA Zheng rong. A method of measuring 2d flow-field at rotor exits of transonic multistage compressor. Journal of propulsion technology, Vol. 34, No. 6, pp 754-759, 2013.

[22] LI Jingyang, MA Hongwei, HE Xiang. Method of measuring 3-D unsteady flow at exits of transonic compressor rotor passages using a two-hole tip-wedge pressure probe. Journal of Aerospace Power, Vol.27, No.10, pp 2262-2268, 2012.

[23] MA Hong wei, WEI Wei, ZHANG Liang, GUAN Hui. Analysis of measured unsteady flow field using a quasi fast response pressure probe. Aeroengine, Vol. 42, No. 2, pp 67-72, 2016.